ORIGINAL RESEARCH

Imaging and Chemical Analysis of External and Internal Ureteral Stent Encrustation

Tal Amitay-Rosen[1], Ishai Dror[2], Yaniv Shilo[3], Brian Berkowitz [2]

[1]Department of Physical Chemistry, Institute for Biological Research, Ness-Ziona, 7410001, Israel; [2]Department of Earth and Planetary Sciences, Weizmann Institute of Science, Rehovot, 7610001, Israel; [3]Department of Urology, Kaplan Medical Center, Affiliated with the Hebrew University of Jerusalem, Rehovot, 7661041, Israel

Correspondence: Brian Berkowitz, Department of Earth and Planetary Sciences, Weizmann Institute of Science, Rehovot, 7610001, Israel, Tel +972-8-9342098, Fax +972-8-9344124, Email brian.berkowitz@weizmann.ac.il

Introduction: Ureteral stents are effective in alleviating flow disruptions in the urinary tract, whether due to ureteral stones, strictures or extrinsic ureteral obstruction. However, significant stent encrustation on the external and/or internal stent lumen walls can occur, which may interfere with stent functioning and/or removal. Currently, there is only limited, generally qualitative, information on the distribution, mineral structure, and chemical content of these deposits, particularly in terms of stent lumen encrustation.

Objective: To quantify, in an initial investigation, external and internal encrustation in representative, intact ureteral stents. The study investigates possible correlations between patterns of external and internal encrustation, determines mineral structure and chemical composition, and examines the potential for stent lumen obstruction even in the absence of external stent wall encrustation.

Study Design: High-resolution, laboratory micro-computed tomography (micro-CT) was used to non-destructively image external and internal stent encrustation in four representative stents. X-ray diffractometry (XRD) and scanning electron microscopy–energy dispersive x-ray spectroscopy (SEM-EDS) enabled parallel analysis of mineral structure and chemical content of samples collected from external and internal encrusted material along the distal, proximal and mid-ureteral stent regions.

Results: Extensive stent lumen encrustation can occur within any region of a stent, with only incidental or minor external encrustation, along the entire length of the stent. External and internal encrusted materials in a given stent are generally similar, consisting of a combination of amorphous (mostly organic) and crystalline mineral deposits.

Conclusion: Micro-CT demonstrates that significant stent lumen encrustation can occur, which can lead to partial or full stent lumen occlusion, even when the exterior stent wall is essentially free of encrusted material.

Keywords: micro-computed tomography, stent deposition, mineral composition, obstruction, stent lumen

Introduction

Ureteral stents are used frequently and effectively to alleviate flow disruptions in the urinary tract, whether due to ureteral stones, strictures or extrinsic ureteral obstruction. Stents are also used following various endourological and other surgical procedures that can affect the ureter, to promote urine flow until edema decreases and incisions heal.

Stents are often subject to mineral deposition: external stent wall and internal stent lumen encrustation can affect stent functioning, interfere with stent removal, and even lead to stent failure.[1,2] However, while mineral deposition is a common occurrence – over both short (weeks) and long (months) durations – only limited studies have analyzed external and internal (stent lumen) encrusted deposits in detail, in terms of both relative amounts and distribution along the stent, as well as mineral structure and chemical content.[3–13] Notably, these studies generally present qualitative descriptions of external encrustation; in only a few cases, limited information is presented on internal encrustation, and/or structure and chemical content of the deposits. From a clinical perspective, though, improvements to stent use and management (eg, timing of stent removal/replacement, imaging and other means to identify rates or likelihood of deposition and occlusion, and choice of stent materials that eliminate deposition) remain largely elusive.

159

The purpose of this study was to test the use of high-resolution, non-destructive, laboratory micro-CT, in an *initial* study, to obtain several detailed maps of stent encrustation patterns – with a focus on the location and amount of stent lumen deposition along stents – and to combine this information with associated SEM-EDS and XRD measurements. In terms of stent function, a particular question of interest is whether a stent lumen remains completely patent when little to no encrustation on the external stent wall is present.

Materials and Methods

Ureteral Stent Collection

Double-J stents (Boston Scientific® Percuflex Plus) were retrieved from 49 (single stent, unilateral) patients undergoing endourological procedures to remove kidney or ureteral stones during the period 2/2019 – 11/2020, with approval of the institutional ethics committees (Kaplan Medical Center, Research No. 0242–18-KMC, and the Weizmann Institute of Science Institutional Review Board, IRB 646–1, and in compliance with the Declaration of Helsinki). In these cases, stents were used either to bypass an obstruction caused by a ureteral stone and/or to facilitate ureter dilatation, prior to endourological stone removal procedures. Informed consent was obtained from the study participants prior to study commencement. Given the computationally intensive nature of the data processing, as well as cost considerations, four stents were subjected to detailed analysis in this initial study. Stent choice was based on visual inspection of the degree of clear external stent wall encrustation, length of time in place, and stent diameter. These stents were chosen because they exhibited varying degrees of external encrustation, as well as varying degrees of occlusion in side holes, the latter of which were assumed to act as indicators of possible internal (stent lumen) encrustation. The choice of stents was intended to facilitate initial appraisal of micro-CT measurements, and the ability to delineate, in particular, internal encrustation features.

No stents contained major deposits or heavy external encrustation (eg, encapsulating the entire pigtail) on the distal or proximal ends of the stents, and none displayed degrees of external wall encrustation on the mid-ureteral region of the stent that inhibited standard stent removal. All stents were removed without patient complications. A stent grasper was used to hold and pull the distal pigtail, without a need to use laser or other means to remove deposits prior to stent extraction. The outer surfaces of the stents were rinsed lightly with saline solution to remove any unattached colloidal debris and urine, immediately upon stent extraction from each patient. Of the four representative stents – labeled #2, #6, #35, #36 – stent #35 was 4.8F diameter, while the other three were 6F diameter. Basic patient information on these stents is given in Table 1.

Micro-Computed Tomography (Micro-CT) Measurements

Micro-CT imaging measurements were performed on the four ureteral stents (#2, 6, 35 and 36), using a laboratory, preclinical ZEISS Xradia 520 Versa microscope; image visualization and analysis were performed using commercial (Avizo) software. Measurements were performed at and above the distal (bladder side) pigtail, along the mid-ureteral

Table 1 Patient/Stent Information

Patient/ Stent No.	Age	Gender	Stent Indwelling Time (Days)	Type of Stone	Prior History of Stones?	Stone Density (Hounsfield Units)	Other
2	54	Male	69	Unknown	No	1270	–
6	39	Female	91	Struvite	No	790	Recurring UTI
35	54	Male	98	Unknown	Yes	800	–
36	71	Male	254	Unknown	No	400	Dialysis[a]

Notes: For all patients, stents were inserted to alleviate obstructed stone located either in the ureter or kidney, prior to subsequent ureteroscopy. [a]Urine cultures indicated presence of Enterococcus faecalis.
Abbreviation: UTI, urinary tract infection.

160

Research and Reports in Urology 2022:14

region of the stent, and below and at the proximal (kidney side) pigtail; voxel size resolution was 13.1 μm. From cross-sectional images (consecutive slices) of encrusted material on the stent external wall and within the stent lumen, the spatial distribution of external stent wall and internal stent lumen encrusted material was determined, in various regions along the stent. In particular, for stents #6, #35 and #36, the degree of stent lumen blockage was determined, calculated as the ratio of cross-sectional areas of stent lumen encrustation to the full stent lumen area in each slice along the length of the stent.

As detailed below, encrusted materials consist of both inorganic and organic deposits, with inorganic material having both crystalline or amorphous structure, and organic material being only amorphous. The micro-CT detects both organic and inorganic material in the stent deposits, independent of crystalline or amorphous structure.

Structural and Chemical Analysis

Detailed measurements were made to analyze separate samples of external and internal encrusted material collected from the distal, proximal and mid-ureteral regions of stents #35 and #36, to characterize the mineral structure and chemical content of the deposits. Six samples taken from each of stents #35 and 36: from 2 cm length beyond the pigtail curl to the stent end, at both distal and proximal sides; middle/center region about 20 cm in length. External encrusted material was collected by scraping the outer stent walls with a blunt edge; internal luminal material was collected by repeated guidewire insertion. For stent #6, because of the limited amount of deposition, two samples were collected (external, internal), from the entire length of the stent. There was insufficient material for chemical analysis of deposits from stent #2. X-ray diffractometry (XRD) provided information on the mineral structure of deposits, particularly in terms of estimates of the fractions of crystalline and amorphous phases. Scanning electron microscopy – energy dispersive spectroscopy (SEM–EDS) provided information on morphology of the deposited material and elemental distributions in selected samples.

Details on the micro-CT, XRD and SEM-EDS measurement methods are contained in the Supplementary Data File.

Results

The four selected stents displayed relatively mild to moderate external encrustation (see Discussion and figures below), according to the order (of increasing degrees of encrustation) #2 < #35 < #36 < #6, and more varying degrees of stent lumen encrustation, according to the order #2 < #6 < #35 < #36. Most discussion of the results is focused on stents #6, #35, and #36, because stent #2 displayed significantly less encrustation than the other three stents. While there were no clinical indications of stent lumen occlusion or other adverse effects in the patients, the degree of external encrustation is delineated because it is important in terms of correlation – or rather, lack thereof – relative to the degree of internal encrustation, as discussed below. In this context, it is meaningful to include reference to stent #2 in the discussion. All four stents showed some degree of relatively smooth brown/black "discoloration" on the external surface, with an increasing degree of surface discoloration in the order #2 < #6 < #36 < #35 (see Discussion below).

Micro-CT Measurements

Figure 1A–D shows the (color-enhanced) spatial distribution of external and internal encrusted material in the *distal* regions of stents #6 and #36. Note the visible occlusions also in some of the stent side holes. The differences in amounts and locations of deposited material between the two stents are significant, both externally and internally. In particular, the degree of external encrustation along stent #6 is relatively high, reaching ~0.5 mm height above the outer wall surface at some locations along the stent. While stent #36 shows far less external encrustation, by comparison, there is significant internal encrustation in the mid-ureteral region portion of the stent, but relatively less in the distal pigtail. From Table 1, it is worth noting that the patient associated with stent #6 had recurrent UTIs, so that biofilm development may have played a role in the encrustation process. In contrast, the stent #36 patient was on dialysis, indicating a low urinary flow rate and urine with a relatively low chemical concentration; in such a case, one might expect a low flow rate within the stent lumen, and facilitation of stent lumen obstruction (see below).

The (color-enhanced) spatial distribution of encrusted material in the *mid-ureteral* regions of stents #6 and #36 is shown in Figure 1E–H. Note that stent #6 displays greater external encrustation, but less internal encrustation, relative to
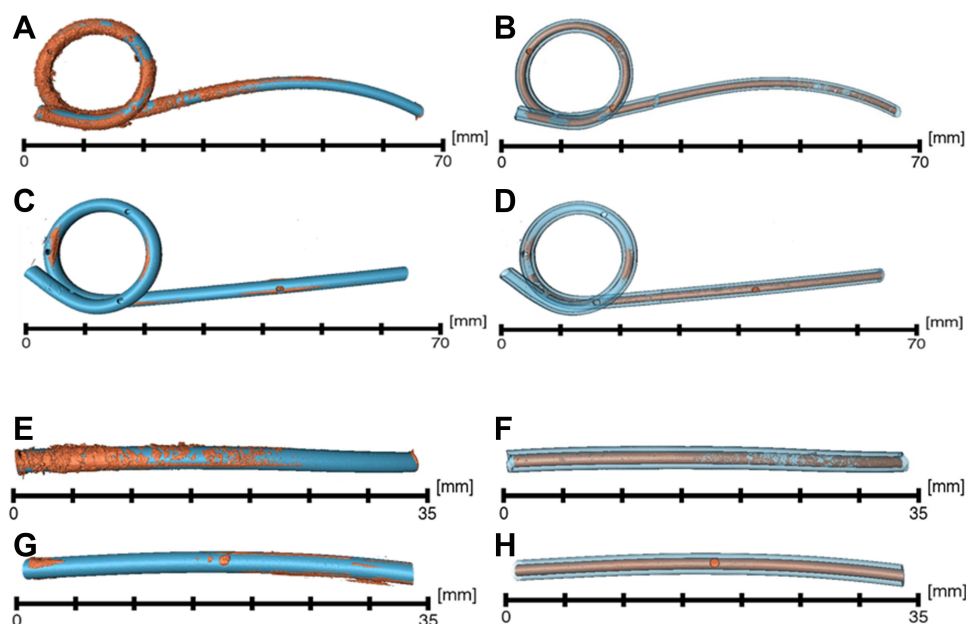
Figure 1 Color-enhanced micro-CT images showing spatial distribution of external and internal encrusted material in the *distal* regions, respectively, of stent #6 (**A** and **B**) and stent #36 (**C** and **D**), and in the *mid-ureteral* regions, respectively, of stent #6 (**E** and **F**) and stent #36 (**G** and **H**). Note the occlusions also in some of the stent side holes. The distal pigtail stent #6 appears more heavily encrusted internally relative to stent #36, although the latter has heavier internal encrustation above the pigtail (see Figure 2), particularly in the mid-ureteral region of the stent.

stent #36. Occlusions in some of the stent side holes are also visible. The measurements for stent #35 are similar to those shown in Figure 1, with somewhat lower external encrustation (#35 < #36 < #6) and intermediate internal encrustation (#6 < #35 < #36); the amounts of both external and internal encrusted deposits along stent #2 are significantly lower.

Figure 2A–C presents the degree of stent lumen blockage, calculated as the ratio of cross-sectional areas of internal encrustation to (clean) stent lumen cross-sectional area, along the region above the distal pigtail in stents #6, #36, and
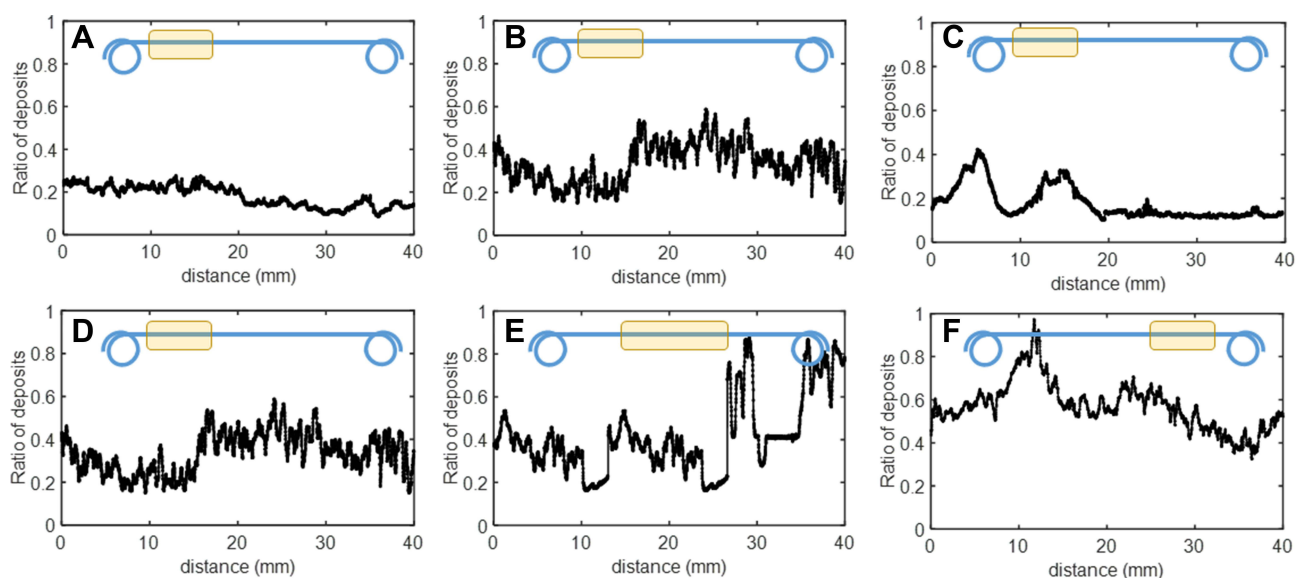

Figure 2 Degree of stent lumen blockage (from stent lumen encrustation) – calculated as the ratio of cross-sectional areas of internal encrustation to stent lumen cross-sectional area along the length of the stent – above the distal pigtail for three different stents: (**A**) stent #6, (**B**) stent #36, and (**C**) stent #35. Also shown are similar ratios along three regions of a single stent, #36, (**D**) above the distal pigtail, (**E**) in the mid-ureteral region, and (**F**) below the proximal pigtail. The schematics show the locations of measurements along the stent.
Note: for clarity and convenience of comparison, plate (**B**) appears also as plate (**D**).

162

Research and Reports in Urology 2022:14

#35. Considerable variability is evident both among stents and along each individual stent. The *maximum* ratios of stent lumen deposits in stents #6, #36, and #35 are, respectively, 0.28 (mean = 0.18±0.05), 0.59 (mean = 0.33±0.10), and 0.42 (mean = 0.18±0.08). Note, too, that these stents displayed relative limited external encrustation in this region, particularly stent #36 (Figure 1).

The degree of stent lumen blockage along the entire length of a single stent is presented in Figure 2D–F, for stent #36, proximal to the distal pigtail region, in the mid-ureteral region, and distal to the proximal pigtail. Again, as seen for Figure 2A–C, wide variability in the amounts of internal encrustation along the stent lumen is found, although there are only a few locations displaying significant external encrustation. The *maximum* ratios of stent lumen material in regions of the stent proximal to the distal pigtail, in the mid-ureteral region, and distal to the proximal pigtail, are, respectively, 0.59 (mean = 0.33±0.10), 0.88 (mean = 0.48±0.17), and 0.97 (mean = 0.57±0.11).

Cross-sectional images of encrusted material (following from Figure 2) are shown in Figure 3A–F, at two locations along the mid-ureteral stent region, in stent #6 (A, B), stent #36 (C, D), and stent #35 (E, F). The relative areas occluded by internal encrustation relative to the stent lumen cross-sectional area are, for (A)-(F), respectively, 0.27, 0.28, 0.8, 0.9, 0.2, and 0.2. This again highlights the relative differences between amounts of external and internal stent encrustation. To further illustrate the potential contrast between amounts of external and internal encrustation, Figure 3G shows the mid-ureteral region of stent #36, cut into 5 pieces to facilitate collection of stent lumen deposits. Significantly, the outer surface has an essentially smooth brown/black coating, with no clear indication of the degree of internal encrustation. However, the inner lumen is heavily occluded with white deposit essentially along the entire length of the stent.

Structural and Chemical Analysis

XRD and SEM-EDS analysis of samples of encrusted material from stents #6, #35, and #36 revealed the following:

Stent #35: The stent contained relatively small amounts of (mostly brown-colored) deposits, being recovered from both external and internal encrustations, in each of the three (distal, mid-ureteral, proximal) regions of the stent. XRD indicated the presence of some externally encrusted calcium carbonate ($CaCO_3$) deposits on the mid-ureteral region of the stent, and amorphous (non-crystalline) material in distal and proximal regions. The bulk of the external and internal deposits consisted of amorphous, non-crystalline (organic and/or inorganic) materials. SEM-EDS confirmed this analysis, and identified that organic matter constituents >90% of all deposited material, with different morphologies observed at the micron level.
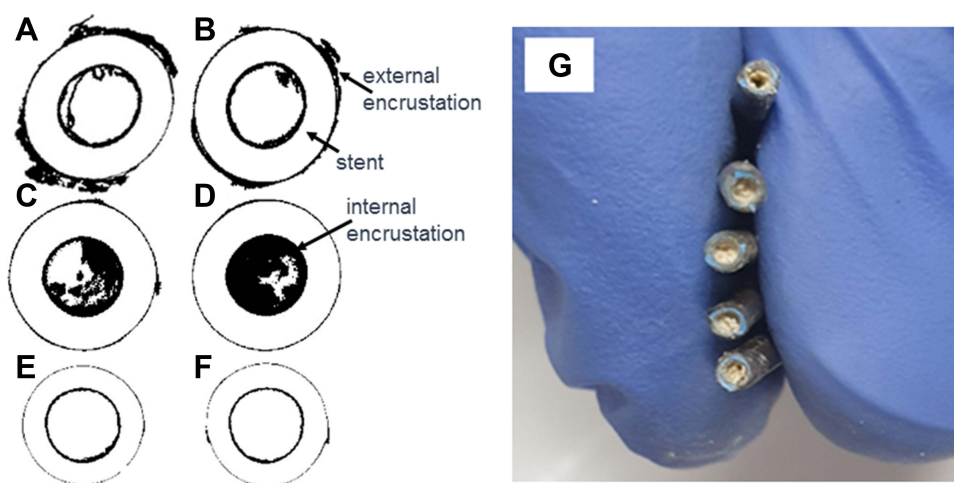

Figure 3 Cross-sectional images of external and internal encrusted material (shown in black), at two locations along the mid-ureteral region of the stent lumen (see Figure 2) in (6F) stent #6 (**A** and **B**), (6F) stent #36 (**C** and **D**), and (4.8F) stent #35 (**E** and **F**). Ratios for (**A–F**) are, respectively, 0.27, 0.28, 0.8, 0.9, 0.2, and 0.2; "ratio" denotes the relative area occluded by internally encrusted material relative to the stent lumen cross-sectional area. Also shown: (**G**) mid-ureteral region of stent #36, cut into 5 pieces to facilitate collection of internally encrusted material. Outer surface – smooth (essentially) brown/black coating, with no clear indication of the degree of stent lumen encrustation. Inner lumen – essentially blocked with white deposit along entire length of stent. Similar observations for proximal and distal regions.

Stent #36: The stent had extensive brown-black discoloration along the entire length of the outer wall, but was otherwise generally smooth, with no externally visible mineral deposition. XRD indicated that the stent contained relatively small amounts of externally encrusted (white-colored) struvite, on each of the three (distal, mid-ureteral, proximal) regions of the stent. Occlusions of all stent side holes also consisted of struvite. Internally, extensive amounts of white-colored material were retrieved, and XRD determined that these deposits, existing on the three stent regions, consisted essentially entirely of struvite. SEM-EDS confirmed this analysis.

Stent #6: The stent contained limited amounts of calcium oxalate (monohydrate), both externally and internally, along the entire length of the stent. SEM-EDS confirmed this analysis.

Discussion

This study offers an initial, detailed quantification of stent external and internal encrustation, and stent lumen encrustation in particular, along the lengths of several stents. As noted in the Introduction, there is currently only limited, generally qualitative, information on the distribution, mineral structure, and chemical content of these deposits, and little reporting of the extent of stent lumen encrustation, which can lead to stent failure.[1–13] A recent study[13] used micro-CT to examine the relative efficacy of stents from two different manufacturers in preventing encrustation. The measurements, at relatively low resolution (with voxel size 8 times larger than those in the current study), focused on determination of overall encrustation volumes in various sections of stents, and did not report relative ratios of stent lumen occlusion along the stents.

The measurements presented here offer several insights. Most significantly, the extent of encrusted material on the stent outer wall yields essentially no indication of the amount and distribution of encrustation within the stent lumen. For example, referring to Figures 1–3, stent #36 showed light external encrustation and heavy internal encrustation, while stent #6 displayed relatively heavy external encrustation and only light internal encrustation; in contrast, stent #2, with little external encrustation, was found also to exhibit little internal encrustation. Indeed, mapping by micro-CT demonstrates that external encrustations can comprise most of the total amount of depositional material on/in the stent. Moreover, the distribution of internal encrusted material along the stent lumen tends to be relatively non-uniform; in some regions (eg, the mid-ureteral region of stent #36; see Figure 2D–F), the local stent lumen encrustation was found to vary from <20% to >90%. Thus, the four stents analyzed here demonstrate wide variations in relative amounts of external and internal encrustation, suggesting that one cannot assume, a priori, that a stent with negligible external encrustation has similarly negligible stent lumen encrustation.

With regard to stent function, relatively high ratios of internal encrustation along the stent lumen may lead to reduction, and even functional loss, in the ability of the stent to conduct and drain urine. To illustrate, referring to stent #36 and Figures 2 and 3, the variability of ratios of internal encrusted material varies locally and widely along the stent, from 33% to 57%, but with *local maximum* ratios reaching as high as ~97%. As such, in this case, the likelihood of a continuous, conducting cross-section of the stent lumen over the entire length of the stent appears low, so that the stent lumen was likely obstructed. In this context, detailed quantitative discussions of the impact of percent stent occlusion on urine flow appear elsewhere.[14,15] These studies[14,15] demonstrate, in particular, that in the presence of external ureteral obstructions, stent lumen occlusion of >90% in even small regions along a stent can lead to significant increases in renal pressure, thus indicating the inability of the stent to conduct urine efficiently.

Note, too, that with internal encrustation, stent side holes can also become largely or completely occluded (as seen, for example, in Figure 1), thus reducing potential urine exchange and flow between the stent and ureter lumina; side hole occlusions are well documented in the literature.[4–10] Of course, even with full occlusion of the stent lumen, kidney drainage can remain normal if urine flow through the ureter lumen, around the stent, remains viable. These findings may explain certain clinical situations, such as patients with an obstructing stone drained with ureteral stent, who develop hydronephrosis and/or urinary tract infection, while imaging does not indicate any evidence of encrustation. In such cases, significant stent lumen encrustation may interfere with and obstruct urine flow, leading to urinary tract infection or renal failure; stent lumen encrustation is not visible by conventional imaging.

Although often designed to avoid or reduce mineral deposition, stents often exhibit substantial encrustation. The chemical content and mineral structure of encrusted deposits, in all (proximal, distal, mid-ureteral) regions of a given stent, appear to

be generally similar, as reported in the literature. However, the type of deposit can vary widely among stents and different patients; for example, stent #35 contains mostly organic material, with only a small amount of externally deposited $CaCO_3$, while stent #36 contains mostly struvite, possibly as a result of infection. It is noted, too, that the chemical and physical properties of stents may change over time. Changes in physical properties include roughness of the stent surface due to various types and amounts of deposition, and side hole blocking. The frequently observed brown-black discoloration along the outer wall of a stent represents one type of chemical change. As demonstrated by Chew et al,[16] this discoloration does not generally indicate surface deposition of crystalline material from urine, but rather reaction between sulfur-containing urinary components and bismuth subcarbonate present in the stent material. One can speculate, though, that such chemical changes to the stent coating may have secondary, longer-term impacts on deposition.

A clinical implication of these findings, though based on a limited number of samples, is that a stent displaying little external encrustation may yet contain significant internal encrustation. The degree of stent lumen encrustation cannot be predicted or determined in advance, for any particular case. As such, and in the absence of any other correlating clinical data, the practice of inserting a guidewire into a previously inserted stent to facilitate guidewire direction to the kidney may result in inadvertent delivery of large amounts of depositional material into the upper urinary tract. Such deposits may act as nucleation material for future kidney stones. Moreover, deposits containing significant amounts of organic/biological constituents (such as for stent #36, which contained mostly struvite) may lead to contamination of the urinary tract and potentially to bacteremia under high renal pressures.

While this initial study examines the relationship between external and internal encrustation by combining micro-CT, XRD and SEM-EDS measurements, several limitations should be noted. First, the four ureteral stents examined in detail are not fully representative of all ureteral stents; comprehensive study can be developed on the proof-of-concept methods and analysis presented here. In addition, factors such as urine chemical composition, duration of stent emplacement, and stent size, style and manufacturer, beyond the scope of this study, are likely to affect encrustation patterns, but could not be correlated here. Similarly, because stone types were generally unknown, it was not possible to correlate encrustation and stone composition.

A future, systematic study on a larger number of stents will allow generalization of the extent of these findings. The methods presented here can enable an effort to correlate measurements of external and internal encrustation amounts, distribution, composition and mineral structure to information on patient history (eg, previous stone occurrences, stone composition, infection, duration of stent emplacement), as well as the type of stent and coating. In particular, it may prove useful to further corroborate the degree of stent lumen encrustation in stents exhibiting minimal external deposits. Future analysis that examines microbial markers, and analysis of stents from patients with other clinical indications, may provide further insights regarding encrustation characteristics. Other studies can focus on the factors leading to non-uniform deposition. It can be speculated that this is due at least in part to variability of precipitation kinetics, as a function of the different residence times (urine velocities and volumes) and time-varying chemical composition of urine in stent and ureter lumina. Shearing/contact between the outer stent wall and ureter wall, and bending of the stent itself, in the course of patient movement, may further reduce or modify deposition patterns.

Conclusions

Micro-CT measurements demonstrate that significant stent lumen encrustation, up to essentially full obstruction, can occur even when the exterior wall and proximal/distal pigtails are essentially free of encrusted material. Associated analysis of mineral structure and chemical content confirms that in each stent, encrusted deposits are generally composed of similar mineral structure and chemical composition, but also that broad variations between external and internal stent deposits occur among patients.

Abbreviations

CT, computed tomography; XRD, x-ray diffractometry; SEM-EDS, scanning electron microscopy – x-ray energy dispersive spectroscopy; ICP-MS, inductively coupled plasma mass spectrometry.

Acknowledgments

Disclosure

The authors report no conflicts of interest for this work.

References

1. Lange D, Bidnur S, Hoag N, Chew BH. Ureteral stent-associated complications—where we are and where we are going. *Nat Rev Urol*. 2015;12 (1):17–25. doi:10.1038/nrurol.2014.340
2. Sali GM, Joshi HB. Ureteric stents: overview of current clinical applications and economic implications. *Int J Urol*. 2020;27:7–15. doi:10.1111/iju.1411
3. Gleeson MJ, Glueck JA, Feldman L, Griffith DP, Noon GP. Comparative in vitro encrustation studies of biomaterials in human urine. *Trans Am Soc Artif Intern Organs*. 1989;35:495–498. doi:10.1097/00002480-198907000-00104
4. Singh I, Gupta NP, Hemal AK, Aron M, Seth A, Dogra PN. Severely encrusted polyurethane ureteral stents: management and analysis of potential risk factors. *Urology*. 2001;58(4):526–531. doi:10.1016/s0090-4295(01)01317-6
5. Kawahara T, Ito H, Terao H, Yoshida M, Matsuzaki J. Ureteral stent encrustation, incrustation, and coloring: morbidity related to indwelling times. *J Endourol*. 2012;26:178–182. doi:10.1089/end.2011.0385
6. Joshi H. Re: ureteral stent encrustation, incrustation, and coloring: morbidity related to indwelling times (From: Kawahara T, Ito H, Terao H, et al. *J Endourol*. 2012;26:178–182). *J Endourol*. 2012;26(7):924–925. doi:10.1089/end.2012.0192
7. Chew BH, Lange D. Re: ureteral stent encrustation, incrustation, and coloring: morbidity related to indwelling times (From: Kawahara T, Ito H, Terao H, et al. *J Endourol*. 2012;26:178–182). *J Endourol*. 2013;27(4):506–507. doi:10.1089/end.2012.0640
8. Kawahara T, Ito H, Terao H, et al. Authors' Response to Chew and Lange, Letter to the Editor: authors' response to Chew and Lange. *J Endourol*. 2013;27(4):507. doi:10.1089/end.2013.1570
9. Sighinolfi MC, Sighinolfi GP, Galli E, et al. Chemical and mineralogical analysis of ureteral stent encrustation and associated risk factors. *Urology*. 2015;86(4):703–706. doi:10.1016/j.urology.2015.05.015
10. Bibby LM, Wiseman OJ. Double JJ ureteral stenting: encrustation and tolerability. *Euro Urol Focus*. 2021;7:7–8. doi:10.1016/j.euf.2020.08.014
11. Legrand F, Saussez T, Ruffion A, et al. Double loop ureteral stent encrustation according to indwelling time: results of a European multicentric study. *J Endourol*. 2021;35(1):84–90. doi:10.1089/end.2020.0254
12. Arkusz K, Pasik K, Halinski A, Halin A. Surface analysis of ureteral stent before and after implantation in the bodies of child patients. *Urolithiasis*. 2021;49:83–92. doi:10.1007/s00240-020-01211-9
13. Yoshida T, Takemoto K, Sakata Y, et al. A randomized clinical trial evaluating the short-term results of ureteral stent encrustation in urolithiasis patients undergoing ureteroscopy: micro-computed tomography evaluation. *Sci Rep*. 2021;11:10337. doi:10.1038/s41598-021-89808-x
14. Amitay-Rosen T, Nissan A, Shilo Y, Dror I, Berkowitz B. Failure of ureteral stents subject to extrinsic ureteral obstruction and stent occlusions. *Inter Urol Nephrol*. 2021;53(8):1535–1541. doi:10.1007/s11255-021-02810-0
15. Amitay-Rosen T, Shilo Y, Dror I, Berkowitz B. Influence of single stent size and tandem stents subject to extrinsic ureteral obstruction and stent occlusion on stent failure. *J Endourol*. 2022;36(2):236–242. doi:10.1089/end.2021.0426
16. Chew BH, Chan J, Choy D, et al. The interaction of urinary components with biomaterials in the urinary tract: ureteral stent discoloration. *J Endourol*. 2020;34(5):608–618. doi:10.1089/end.2019.0551